processes

MDPI

Article

Gas Desorption Characteristics of Different Coal Ranks

Huigang Xu [1,2], Xuyao Qi [1,2], Haidong Wang [3,*], Zhongqiu Liang [4], Tao Yang [3], Yongming Zou [4], Qi Jiang [3] and Lei Jin [3]

[1] School of Safety Engineering, China University of Mining and Technology, Xuzhou 221116, China; xhg20240115@163.com (H.X.)
[2] Key Laboratory of Gas and Fire Control for Coal Mines, China University of Mining and Technology, Xuzhou 221116, China
[3] School of Safety Engineering, North China Institute of Science & Technology, Langfang 101601, China
[4] CCTEG Shenyang Research Institute, Shenyang 113122, China
* Correspondence: whd@ncist.edu

Abstract: It is crucial to understand the desorption and diffusion characteristics of coal seam gas to prevent gas disasters in coal mines. This study conducted constant-temperature gas dispersion tests on lignite, fiery coal, and anthracite to uncover the complexities of gas diffusion in coal samples under the influence of coal metamorphism. The main focus was on determining their gas desorption and diffusion characteristics and analyzing the mathematical models of gas dispersion for coal samples with varying degrees of metamorphism over different durations. The results indicated that highly metamorphosed coal samples reached the desorption limit quickly, while low-rank lignite required more time to reach the limit. The gas desorption diffusion rate was notably sensitive to the level of coal metamorphism. In the first 10 min, the gas desorption rate remained stable for lignite and fiery coal, whereas anthracite exhibited a rapid desorption rate in the initial 4 min followed by stability in the subsequent 6 min. Additionally, the effective gas diffusion coefficient showed a strong negative linear correlation with the degree of metamorphism, indicating reduced gas diffusion ability with increased metamorphism. The empirical formulas applied to anthracite showed stable correlation indices, with Formula 3 considered more suitable for describing the gas desorption processes of lignite and fiery coal.

Keywords: coalbed methane (CBM); desorption; diffusion; degree of metamorphism

check for updates

Academic Editor: Raymond Cecil Everson

Received: 19 December 2024
Revised: 5 February 2025
Accepted: 8 February 2025
Published: 18 February 2025

Citation: Xu, H.; Qi, X.; Wang, H.; Liang, Z.; Yang, T.; Zou, Y.; Jiang, Q.; Jin, L. Gas Desorption Characteristics of Different Coal Ranks. *Processes* **2025**, *13*, 570. https://doi.org/10.3390/pr13020570

Copyright: © 2025 by the authors. Licensee MDPI, Basel, Switzerland. This article is an open access article distributed under the terms and conditions of the Creative Commons Attribution (CC BY) license (https://creativecommons.org/licenses/by/4.0/).

1. Introduction

China's energy is characterized by its rich coal resources, poor oil resources, and little gas. Its proven coal reserves account for 33.8% of the world's coal reserves [1,2]. With the increase in mining depth, the ground stress and gas pressure of coal seams increase, and dynamic gas disasters in coal mines become more and more serious [3–5]. Studying the desorption and diffusion characteristics of gas not only has an important impact on the development of coalbed methane resources but also forms the theoretical basis for the prevention of gas disasters in coal mines. Gas desorption and adsorption are mutually reversible processes that can also be called mass transfer processes [6–8]. In the process of coal adsorption and desorption, there are some complex mechanisms of change, such as the effects of temperature and pressure, which also affect the adsorption and desorption performance of coal [9,10]. China's energy profile is defined by its abundant coal, limited oil, and scarce gas resources. The country's proven coal reserves make up 33.8% of the global total. As mining depth increases, the ground stress and gas pressure in coal seams rise, leading to more severe dynamic gas disasters in coal mines [3–5]. Research on the desorption and

diffusion characteristics of gas not only significantly impacts the development of coalbed methane resources but also forms the theoretical basis for preventing gas disasters in coal mines [6–8]. Gas desorption and adsorption are reversible mass transfer processes that play a crucial role in coal adsorption and desorption, with complex mechanisms influenced by factors such as temperature and pressure, ultimately affecting the performance of coal in adsorption and desorption processes [9,10].

Different ranks of coal possess varying structures, leading to differences in their desorption capacities. The Langmuir adsorption constant of coal, determined by analyzing pore distribution characteristics, can accurately predict gas content and pressure in coal seams [11–14]. This constant also aids in assessing the risk of coal and gas outbursts and predicting their likelihood. It serves as a vital parameter for evaluating the surface adsorption capacity of coal, influenced by internal factors such as the coal metamorphism degree, rock composition, test conditions, and parameter settings [15–17].

In coal containing gas, free and adsorbed gasses reach a dynamic equilibrium, and any changes in gas pressure, temperature, shocks, or oscillations lead to the establishment of a new equilibrium state [18,19]. According to Yang et al. [20], the initial effective diffusion coefficient during gas desorption is linked to factors like the pressure, temperature at adsorption equilibrium, and coal sample particle size. Pores play a critical role in gas adsorption, desorption, seepage, and diffusion, impacting the diffusion rate, adsorption capacity, and desorption capacity of gas, thus influencing production efficiency. Li et al. [21] discovered that as the structural damage in coal gradually increases, changes occur in pore volume and specific surface area. The ratio of large and mesoporous pores increases gradually, while the ratio of micropores decreases gradually. Upon reaching a certain level of structural damage, the volume ratios of large and mesopores undergo changes, whereas the volume ratio of micropores remains stable.

Furthermore, the structure of large and medium pores can lower the gas osmotic pressure and decrease its diffusion rate, thereby enhancing gas desorption efficiency effectively [22]. Gasparik, M. et al. [23] conducted a comprehensive study on the influence of coal rank on coalbed methane desorption, exploring changes in saturation adsorption capacity and adsorption curve during desorption. Kusuma, M.I. et al. [24] utilized molecular dynamics simulation to investigate the impact of the coal rank on coalbed methane desorption, offering theoretical insights into the interaction between adsorbent and gas and desorption rate during the process. Kang et al. [25] observed that shorter micropores in coal lead to a reduced gas migration distance within the coal body, shorter transport time, and higher initial-stage adsorption capacity. Hu et al. [26] noted that with increased coal metamorphism, the significance of large pores in gas desorption and diffusion laws diminishes, while the influence of micropores grows.

To date, researchers have compared and tested coal adsorption and desorption behaviors in various mining regions and with different coal ranks, establishing the corresponding relationships. These studies involve analyzing factors such as the coal metamorphism degree, reservoir pressure, temperature, coal rank, and water content. Among these factors, the coal rank notably impacts the adsorption and desorption capacity, with the adsorption capacity decreasing as the coal rank increases. However, limited research has focused on the gas desorption and diffusion characteristics of coals with varying metamorphism degrees, and a unified mathematical expression for gas desorption is lacking. To address this gap, desorption tests were conducted on coals with different metamorphism degrees, employing a more extensive mathematical formula to fit gas desorption curves and deriving gas release patterns for coals with varying metamorphism degrees. These findings will serve as a valuable reference for coal mine safety.

2. Methodology

2.1. Sample Preparation

The experimental samples included lignite from Anjialing Coal Mine, fiery coal from Yushuling Coal Mine, and anthracite from Xinyuan Coal Mine, as shown in Figure 1. After sampling, the coal samples to be measured were broken, crushed, and screened, respectively. Experimental coal samples with a particle size of 0.20–0.3 mm were screened and placed in the oven for 6 h, and the drying temperature was 70 °C. Then, the samples were allowed to stand and cool down to 21 °C, sealed, and stored until being used.

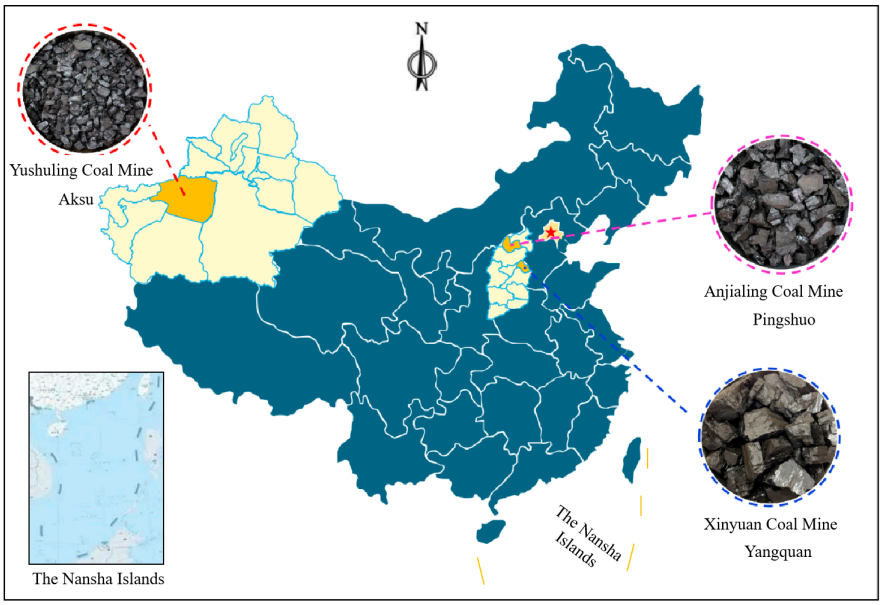


Figure 1. Geographical locations of the coal samples.

According to the parameters obtained through an industrial analysis, all experimental coal samples were reduced to a 1–3 mm particle size for use, dried in a drying oven at 70 °C for 6 h, cooled to 21 °C, and sealed until being used. The related gas parameters and maximum vitrinite reflectance of the selected coal samples are shown in Table 1 (according to GB/T212-2008, GB/T40485-2021) [27,28].

Table 1. Coal quality analysis and related gas parameters of mines.

Coal Mine	Coal Variety	M_{ad}/%	A_d/%	V_{daf} /%	Porosity /%	a /($m^3 \cdot t^{-1}$)	b /MPa	$R_{0,max}$ /%
Anjialing	Lignitic	1.09	16.34	34.25	3.83	8.975	1.146	0.308
Yushuling	Fiery coal	1.10	5.31	41.13	3.82	13.914	1.258	0.721
Xinyuan	Anthracite	1.76	13.09	7.02	0.13	40.546	1.147	2.382

M_{ad} is moisture, A_d is ash, V_{daf} is a volatile, a and b are the Langmuir adsorption constants, and $R_{0,max}$ is the maximum vitrinite reflectance.

2.2. Test Method

2.2.1. Scanning Electron Microscopy

The pore morphology of the coal surface was determined by scanning electron microscopy (SEM), which revealed the morphology characteristics of micrometer cracks and large pores on coal surface through high-magnification optical photography. During the experiment, the appropriate amount of coal sample was uniformly glued to the special base. Due to the poor electrical conductivity of the coal, it was necessary to spray gold to prevent the accumulation of static electricity and improve the imaging contrast. After that,

an FEIQuantaTM250 scanner electron microscope was used to observe the development of pore cracks on the surface of coal samples by using a high-vacuum mode.

2.2.2. Low-Temperature Nitrogen Adsorption

Both the MIP and N_2GA methods have advantages in the characterization of coal pore structures. While the former is capable of measuring the distributions of pores of all sizes, its accuracy for minipores and micropores is low due to pressure damage. Thus, N_2GA is the better choice.

The N_2GA test was carried out with a Quantachrome NOVA-4200e specific area and pore size analyzer, which is designed for static physical adsorption–high-purity (99.999%) nitrogen adsorption–desorption in a liquid nitrogen environment (77.3 K) and is applicable to pores between 0.35 and 500 nm in diameter (according to "Pore size distribution and porosity of solid materials by mercury porosimetry and methane adsorption, Part 1: Mercury porosimetry" (GB/T 21650.1-2008) [29]. The N_2GA test was carried out with a Quantachrome NOVA-4200e specific area and pore size analyzer, which is designed for static physical adsorption–high-purity (99.999%) nitrogen adsorption–desorption in a liquid nitrogen environment (77.3 K) and is applicable to pores between 0.35 and 500 nm in diameter.

2.2.3. Gas Isothermal Adsorption and Desorption Test

This experiment was carried out using an independently developed isothermal adsorption and desorption system that consisted of six main parts: a gas supply and gas control system, adsorption and desorption system, pressure collection system, vacuum degassing system, temperature measurement system, and desorption gas collection system. The test pressure range was 0–6 MPa, as shown in Figure 2.

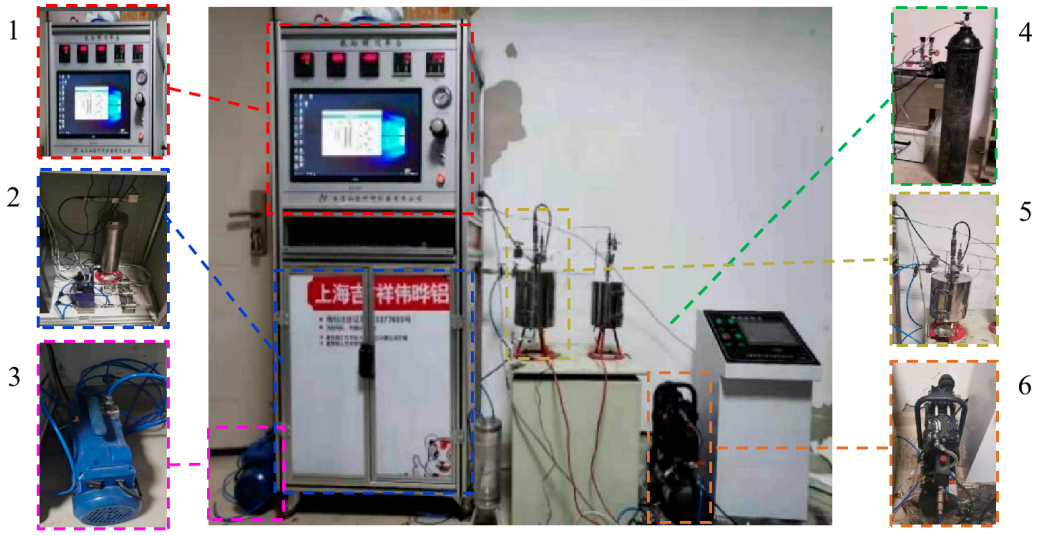


Figure 2. Isothermal adsorption desorption system. 1, computer acquisition system; 2, reference tank; 3, vacuum pump; 4, gas cylinders; 5, coal sample tank; 6, vacuum pump.

In order to study the adsorption–desorption kinetic characteristics of three coal samples under different gas pressures, 99.99% CH_4 was used to carry out the test, and three different gas pressures were set, which were 0.74 MPa, 1.06 MPa, and 1.46 MPa. In order to avoid the chance of bias in the test results, three groups of experiments were carried out in each scheme, and one group of data was selected for analysis when there was no large error in the experimental results. The specific test steps were as follows:

(1) In the preparation stage of the experiment, an air tightness test was carried out first.

(2) Then, 300 g of the coal sample was placed in an adsorption tank. The constant temperature water bath system and vacuum pump were turned on at the same time, with the degassing the sample to be tested in a constant-temperature water bath at 60 °C for 12 h and the removal the water and gas from the coal sample until the air in the coal sample reached the vacuum degree of 4 Pa.

(3) Gas was injected into the tank with the coal sample at a preset pressure, constant-pressure adsorption was maintained for 24 h, and it was ensured that the internal temperature of the adsorption tank was less than room temperature.

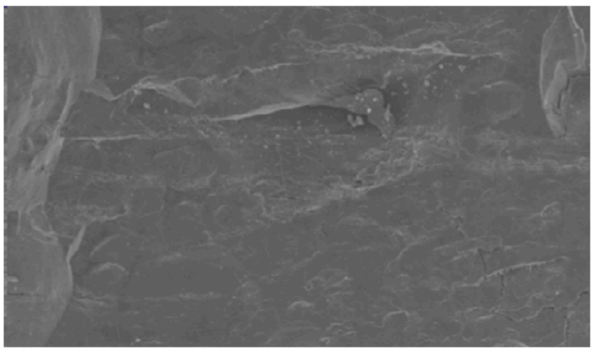
(4) Tests were conducted according to the GB/T19560-2008 standard [30], and desorption data were continuously recorded every 5 s for more than 100 min.

3. Results and Discussion

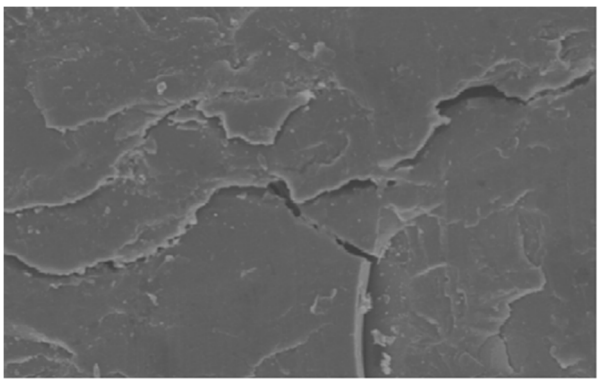
3.1. Coal Sample Pore Structure

3.1.1. SEM

It can be seen from Figure 3 that the Anjialing, Yushuling, and Xinyuan coal samples all have obvious fractures and better pore development. By comparing the scanning electron microscope images of the three coal samples, it can be found that the surface of Anjialing coal samples is the most flat, and most of the cracks are brittle tensile cracks or shear cracks in the shape of a cross. The flatness of the Yushuling coal sample is the second-highest; the fracture morphology and pore morphology are similar to that of the Shuangliu coal sample, but the mineral particle filling is more obvious. The surface of the Yushuling coal sample has a large number of scaly structures and a large number of pyrolytic pores. From the above characteristics, it can be concluded that the pore development status of experimental coal samples is basically as follows: Anjialing < Yushuling < Xinyuan. This result can be explained by the relationship between coal metamorphism and porosity.

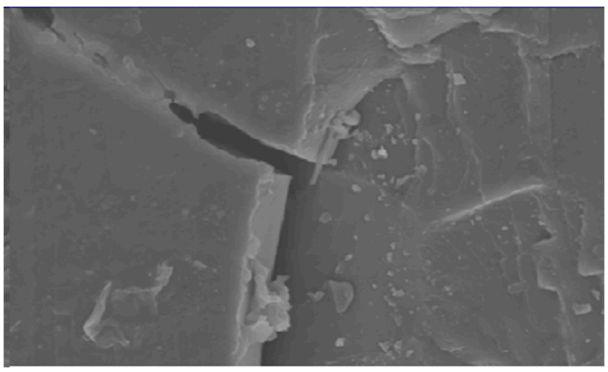


(**a**) Anjialing.



(**b**) Yushuling.

Figure 3. *Cont.*



(**c**) Xinyuan.

Figure 3. SEM results of three coal samples. (**a**) Anjialing; (**b**) Yushuling; (**c**) Xinyuan.

3.1.2. N_2GA

It can be seen from Figure 4 that the gas adsorption volumes of the three coal samples are 2.04 cm^3/g, 3.87 cm^3/g, and 5.85 cm^3/g, respectively. The adsorption capacity of anthracite is higher than that of fiery coal and lignite, and the adsorption capacity of fiery coal is higher than that of lignite, indicating that the adsorption capacity of coal increases with an increase in coal metamorphism. There are hysteresis loops in all three types of coal, indicating that all coal contains open pores. Lignitic coal has the smallest hysteresis loop and is not closed, and the inflection points of adsorption and desorption curves are not obvious, and the adsorption isotherms and desorption isotherms basically coincide. This phenomenon indicates that a cylindrical shape with one end closed and a slit shape with four sides open are common in this rank of coal. Fiery coal has large hysteresis loops, many open and breathable pores, and good pore connectivity. The adsorption and desorption curves roughly coincide, and the adsorption and desorption curves basically coincide with the higher and lower sections of relative pressure, indicating that there are many semi-closed pores and open and breathable pores in its interior. The adsorption isotherm and desorption isotherm of anthracite show a separate state and do not close at the stage of relatively low relative pressure, which indicates that anthracite has a high degree of micropore development and is dominated by cylindrical micropores with one end closed, and the pore connectivity is poor.

As one of the important observation indicators of pore structure characteristics in coal, the pore size distribution can directly reflect the pore structure characteristics. The pore size distribution of coal based on BJH method analysis is shown in Table 2.

Table 2. Pore size distribution of test coal samples.

Coal Variety	Diameter/nm	Cumulative Pore Volume/($cm^3 \cdot g^{-1}$)	Percentage/%
Lignitic	<10	0.0021	55.3%
	10–100	0.0011	28.9%
	>100	0.0006	15.8%
Fiery coal	<10	0.003875	65.3%
	10–100	0.001205	20%
	>100	0.0000860	14.7%
Anthracite	<10	0.0079	80%
	10–100	0.00131	13.3%
	>100	0.000665	6.3%

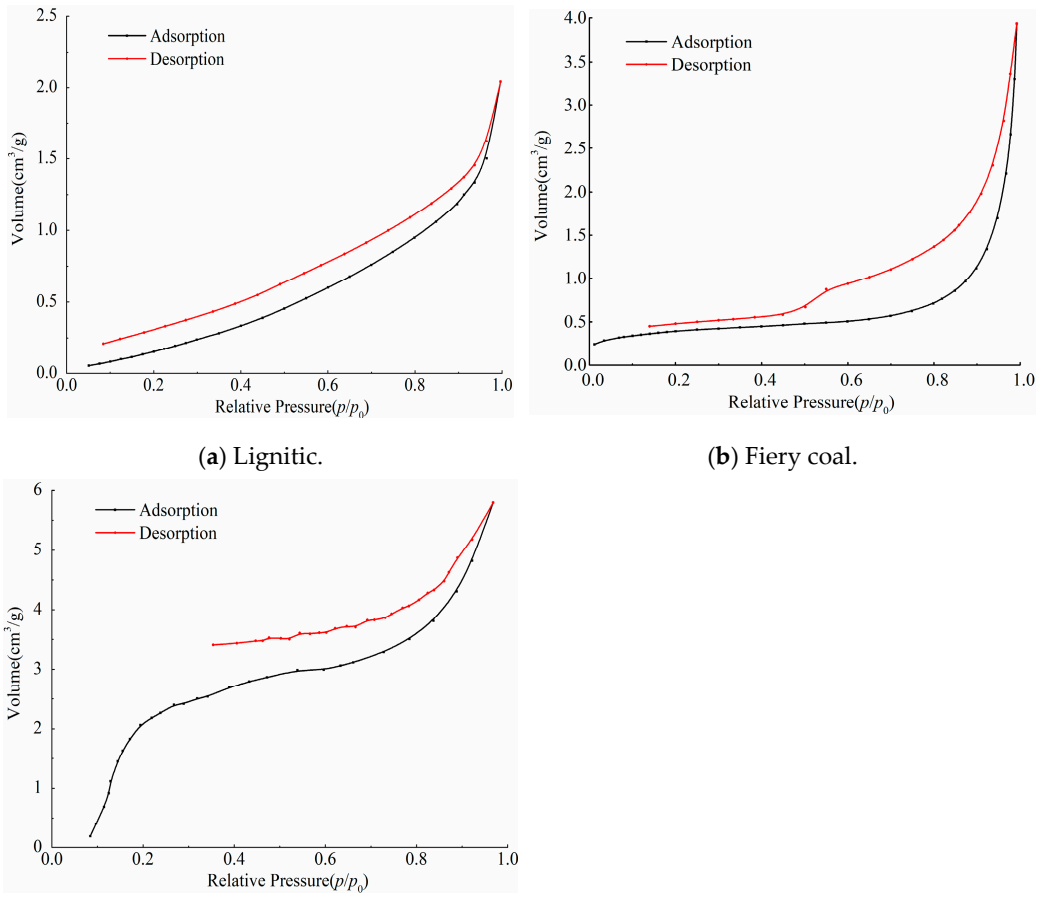


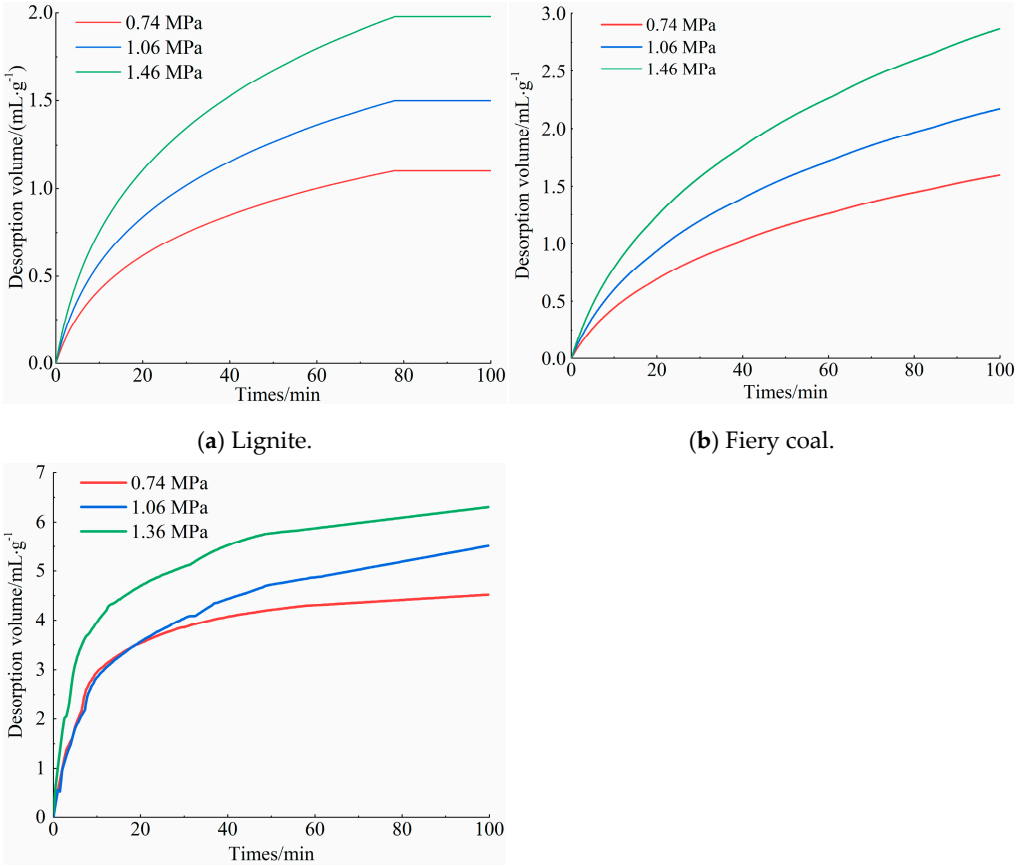
Figure 4. N_2GA adsorption and desorption isotherms of coal samples. (**a**) Lignitic; (**b**) Fiery coal; (**c**) Anthracite.

3.2. Influence of the Degree of Metamorphism on the Amount of Gas Desorption in Coal

Figure 5 presents the Q-t isothermal gas desorption curve of coal samples with different metamorphic degrees at various gas equilibrium pressures over a 100 min period. It is evident that, under consistent external environmental conditions, the cumulative gas desorption from coal increased gradually as the desorption time was extended. Once reaching a certain threshold, the cumulative gas desorption showed minor fluctuations around a stable value. Notably, regardless of the desorption time, the curves obtained under high pressure consistently exceeded those obtained under low pressure, indicating that a higher equilibrium pressure correlated with greater cumulative gas desorption.

During the initial phase of gas desorption, the amount of desorbed gas increased with the degree of coal metamorphism. Highly metamorphic coal samples exhibited a more pronounced increase in gas desorption. For lignite, gas desorption increased with rising pressure. The first 10 min of desorption displayed the highest gas desorption amount and rate, representing a rapid desorption stage. Subsequently, the desorption rate stabilized gradually, and gas desorption showed a slow increase, marking the onset of a stable desorption stage at around 80 min. Similarly, fiery coal showed increased gas desorption with pressure increments. The highest desorption amount occurred within the first 5 min, accompanied by a relatively high desorption rate, indicating the rapid desorption stage. Beyond 5 min, while the desorption amount continued to increase gradually, the desorption rate slightly decreased, signaling the beginning of a stable desorption stage. Anthracite's desorption capacity also varied with pressure changes, increasing as the pressure rose. The most substantial gas desorption took place within the initial 10 min, with the highest

desorption rate, representing the rapid desorption stage. After 10 min, the desorption rate stabilized gradually, and gas desorption increased slowly, entering a stable desorption stage. These observations provide valuable insights into the desorption characteristics of different coal samples under varying pressures, delineating distinct stages of rapid and stable desorption.



(**a**) Lignite. (**b**) Fiery coal.

(**c**) Anthracite.

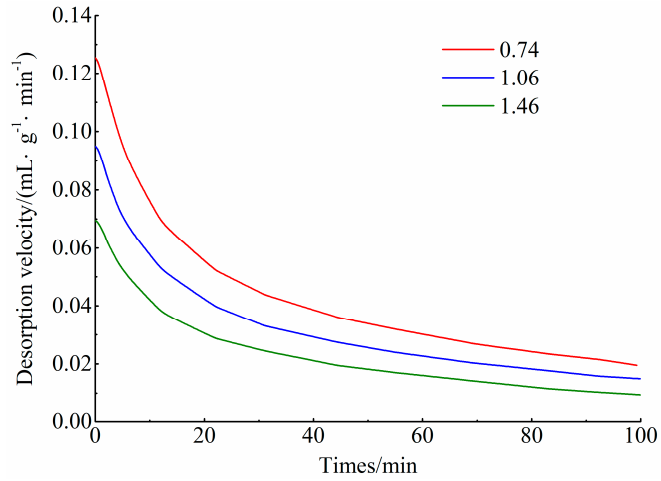
Figure 5. Coal desorption curve. (**a**) Lignite; (**b**) Fiery coal; (**c**) Anthracite.

The most significant gas desorption characteristics of the coal occurred within the initial 3 min. Considering the degrees of metamorphism, the cumulative desorption amounts of the three coal samples (lignite, fiery coal, and anthracite) within the first 10 min represented 76.1%, 45.2%, and 36.7% of the total desorption, respectively. This indicates that coal samples with higher metamorphic degrees reached the limiting value comparatively quickly, while low-rank lignite required a longer time to reach the limit. However, with prolonged desorption time, the gas desorption rate of highly metamorphic coal samples showed a progressively faster decline, leading to a subsequent deceleration in the desorption rate.

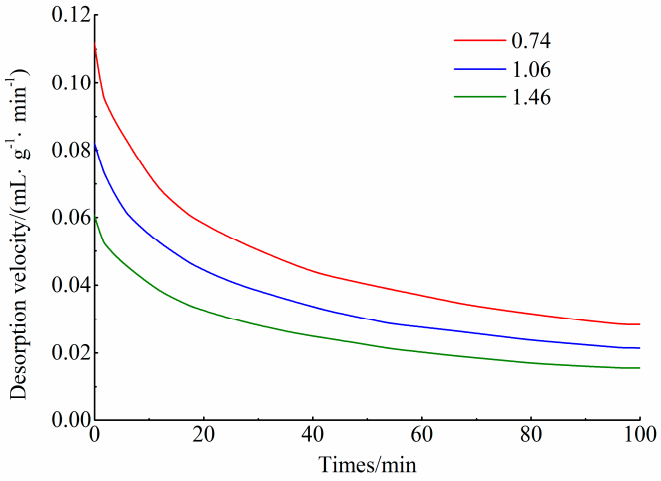
3.3. Effect of the Metamorphic Degree on the Gas Desorption Rate of Coal

The changes in the desorption rates of the three coals over time are depicted in Figure 6. It is evident that the trends in the changes in desorption velocities differed among the three coal ranks. However, the initial gradient of the curve under high pressure was greater than that under low pressure, indicating a higher initial gas desorption velocity under high equilibrium pressure compared to low equilibrium pressure. Additionally, the maximum gas desorption rate under different pressures and the rate of decline in the desorption rate varied with the degree of coal metamorphism. Among the three coal samples, anthracite,

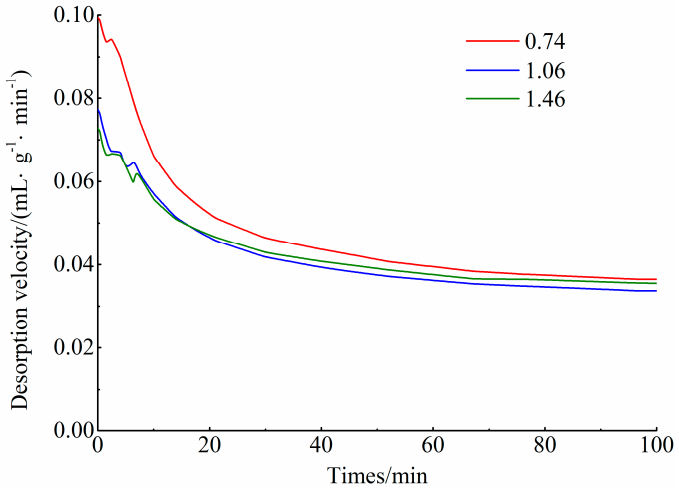
which had the highest coal rank, exhibited the smallest initial gas desorption velocity when the equilibrium pressure ranged from 1.36 to 1.46 MPa. However, as the desorption process progressed, its desorption velocity decreased and became the slowest within the same time frame.



(**a**) Lignite.



(**b**) Fiery coal.



(**c**) Anthracite.

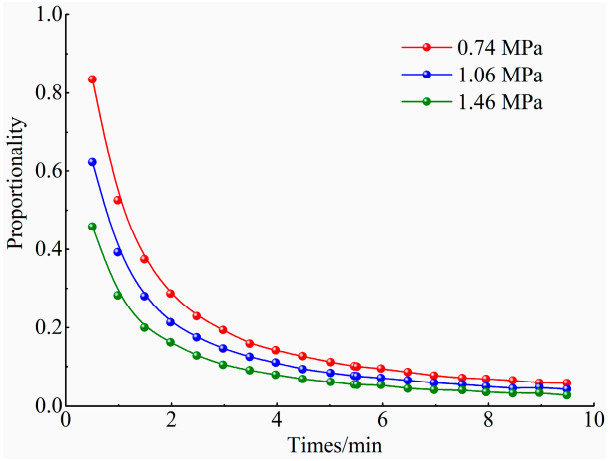
Figure 6. Changes in the desorption rate of coal under various gas equilibrium pressures are examined. (**a**) Lignite; (**b**) Fiery coal; (**c**) Anthracite.

The initial desorption rate of the low metamorphic fiery coal was low, and it gradually decreased as the desorption process continued. Among the three coal samples, lignite, with the lowest degree of metamorphism, exhibited the highest initial gas desorption rate, but it also experienced the fastest subsequent decline. Specifically, when the equilibrium pressure was 1.06 MPa, low-rank lignite displayed the fastest initial gas desorption rate, which swiftly decreased as the desorption progressed. On the other hand, gassy coal, with a metamorphic degree intermediate to the other coal samples, demonstrated a relatively faster initial gas desorption rate, which gradually decreased over time. Anthracite had the lowest initial gas desorption rate, and its desorption speed decreased the slowest over the same duration.

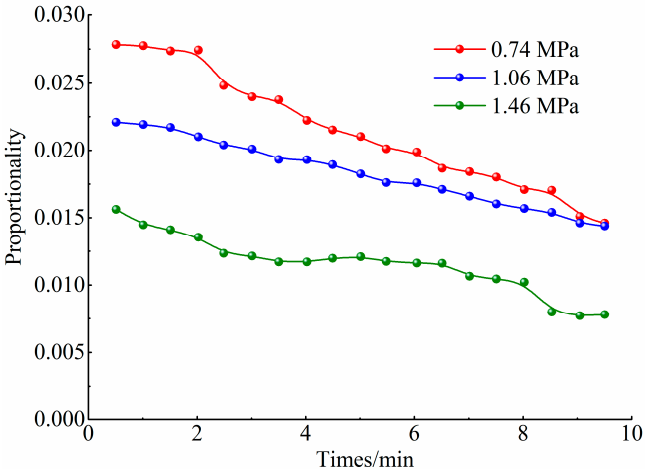
When the equilibrium pressure was 0.74 MPa, the intermediate metamorphic fiery coal exhibited the smallest initial desorption rate. As the desorption process continued, the desorption rate slowly decreased over the same duration. Remarkably, the initial desorption rate of anthracite, with a high degree of metamorphism, did not differ greatly

from that of lignite, which had the lowest degree of metamorphism. However, as the desorption process continued, anthracite experienced the smallest decrease in desorption rate over the same duration, while lignite exhibited the greatest decline.

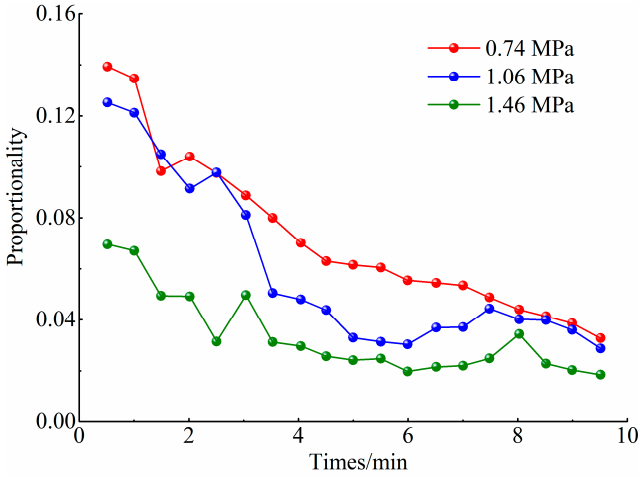
Data were collected at half-minute intervals during the initial 10 min, and a curve was plotted based on the difference between the former and latter groups. The ratio of the former group's desorption rate to the latter group's is presented in Figures 7 and 8. It is evident from these Figures that the desorption rate curves for the three experimental coals exhibited distinct trends. The difference in desorption rate within the first 10 min under varying pressures was more pronounced for lignite compared to fiery coal and anthracite, implying a greater decline in desorption rate for lignite. Furthermore, the difference in desorption rate for lignite within the initial 10 min showed no significant variation between the first 4 min and the last 6 min, while the difference in desorption rate for fiery coal did not significantly differ from that of the last 6 min. The linear correlation between the ratio of differences in the desorption rate within the first 4 min was stronger than that of the last 6 min, and the linear correlation coefficient increased with the increase in gas pressure.



(**a**) Lignite.



(**b**) Fiery coal.



(**c**) Anthracite.

Figure 7. Proportionality of the desorption rate of coal under different gas pressures. (**a**) Lignitic; (**b**) Fiery coal; (**c**) Anthracite.

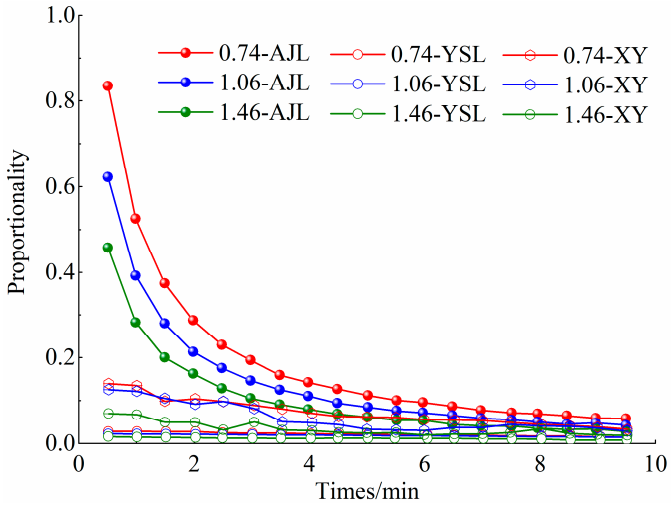


Figure 8. Summary of the desorption rates of coal under different pressures.

3.4. Effect of the Metamorphic Degree on the Gas Diffusion Characteristics of Coal

After undergoing the processes of adsorption and desorption, gas permeates the pores of the coal matrix. By utilizing desorption data and applying Fick's second law of diffusion, it is possible to calculate a physical parameter that characterizes the gas diffusion capacity within coal, known as the effective diffusion coefficient. Through linear regression analysis between the effective diffusion coefficient and the maximum reflectance of vitrinite, the impact of the degree of metamorphism on gas diffusion performance can be examined. The diffusion coefficient signifies the ability of coal to facilitate gas diffusion, and its numerical value reflects the rate at which gas migrates through coal pores. In this study, the effective diffusion coefficient was introduced as a means of quantifying the gas diffusion capacity. The relevant expressions are provided below:

$$\frac{Q_t}{Q_\infty} = 1 - \frac{6}{\pi^2}\sum_{n=1}^{\infty}\frac{1}{n^2}exp(-n^2\pi^2 D_e t) \tag{1}$$

$$Q_\infty = \left(\frac{abp}{1+bp} - \frac{abp_0}{1+bp_0}\right)[1 - M_{ad} - A_{ad}] \tag{2}$$

where Q_t is the amount of gas desorption from coal at time t (mL/g); Q_∞ is the limiting gas desorption capacity of coal (mL/g); t is the desorption time (s); D_e is the effective diffusion coefficient (s^{-1}); p_0 is the gas pressure during the test (MPa); and M_{ad} and A_{ad} are the moisture and ash in coal (%).

The direct determination of the effective gas diffusion coefficient using the formula mentioned above is not feasible. To address this, we set $n = 1$ in Equation (1) and performed a logarithmic transformation of both sides of the equation, thus converting it into a linear fitting formula for the calculation.

$$\ln\left(1 - \frac{Q_t}{Q_\infty}\right) = -\frac{\pi^2 r^2 D_e}{a^2}t + ln\frac{6}{\pi^2} \tag{3}$$

Here, $-\frac{\pi^2 r^2 D_e}{a^2}$ is $\ln\left(1 - \frac{Q_t}{Q_\infty}\right)$ in the linear fitting slope of the curve. The effective gas diffusion coefficients of the three coal samples were then calculated through inverse fitting, and the calculated results are shown in Table 3.

Table 3. Effective gas diffusion coefficients of the coal samples.

Coal Samples	Lignite	Fiery Coal	Anthracite
D_e/s^{-1}	9.32×10^{-5}	6.18×10^{-5}	0.36×10^{-5}

The effective diffusion coefficients of the coal samples, as shown in Table 3, followed a descending order: lignite, fiery coal, and anthracite. This observation markedly contrasts with the pre-desorption amount and adsorption constant of the coal samples mentioned earlier, suggesting that the impact of metamorphism on the gas diffusion capacity differs significantly from its influence on the adsorption and desorption capacity.

The relationship between the effective gas diffusion coefficient and the metamorphic degree of the coal samples was calculated based on the measured results for the maximum reflectivity of vitrinite and the effective gas diffusion coefficients. Figure 9 demonstrates this relationship. Figure 9 shows that there is a strong negative linear correlation between the effective gas diffusion coefficient and the maximum reflectance of vitrinite, indicating that the ability of gas to diffuse in coal decreases as the metamorphic degree increases. The variation in effective gas diffusion coefficients among coal samples with different degrees of metamorphism can be primarily attributed to the maceral components of the coal itself, as well as compaction and dehydration during the coalification process. Coals with a lower degree of metamorphism tend to have a higher content of inertinite and chitinite at the maceral level, resulting in abundant large pores within these macerals. These pores provide ample space for gas diffusion, facilitating the gas diffusion process.

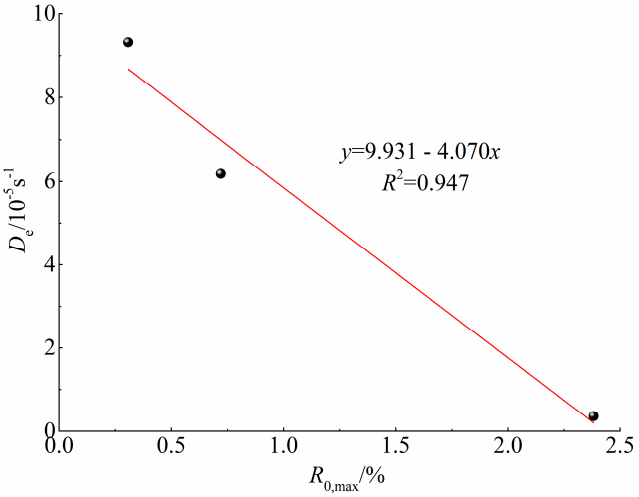


Figure 9. Relationship between the effective diffusion coefficient and the degree of metamorphism in coal.

It can be seen from the above research that the more developed the pore structure of the coal sample, the stronger the corresponding desorption capacity. Because the pore structure of medium and large pores is more developed, it can provide a larger surface area and permeability, which can adsorb and desorb gas more effectively. At the same time, coal gas adsorption and desorption represent a reversible process, and the stronger the desorption capacity, the faster the corresponding gas adsorption speed. The analysis of the pore structure characteristics of coal samples combined with low-temperature liquid nitrogen adsorption experiments also confirmed that the gas adsorption capacity of AJL and YSL coal samples was significantly lower than that of XY coal samples. With the poor opening of micropores in coal samples, gas is not easily dispersed from micropores to large pores. With the increase in pores, once gas is released to large pores, it is very

easily dispersed to the outside world due to the good opening of large pores. In the initial stage of gas desorption, gas desorption is difficult, so it is preferred to desorption in large pores. XY coal samples have more micropores and poor connectivity, so the decrease in gas desorption rate is uneven and large, while AJL coal samples have more large pores, so the overall decrease trend in the desorption rate in the first 10 min is stable. Based on the relationship between pore structure and gas adsorption and desorption ability in coal of different coal ranks, it can be concluded that micropore structure plays a decisive role in gas adsorption ability, while the development degree of medium and large pores plays a decisive role in gas adsorption balance and rapid desorption ability, and there is a positive correlation between them.

4. Gas Desorption Dynamics Models

Numerous studies by domestic and foreign scholars have focused on the mathematical modeling of gas desorption in coal, resulting in the proposal of various formulas. However, some of these formulas have limitations. To investigate the gas desorption behavior of the three coal samples and identify suitable mathematical expressions, a commonly employed formula was utilized to fit the desorption process under different pressures. The mathematical expressions employed are presented in Table 4.

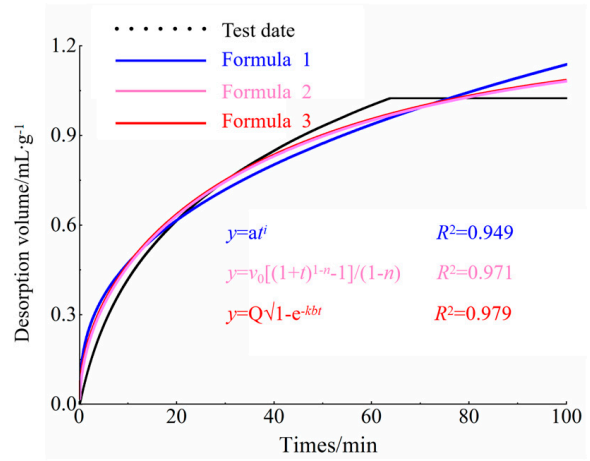
Table 4. Mathematical expression for gas desorption fitting.

NO.	-
Formula 1	$Q_t = at^i$
Formula 2	$Q_t = v_0\left[(1+t)^{1-n} - 1\right]/(1-n)$
Formula 3	$Q_t = Q_\infty\sqrt{1-e^{-kbt}}$

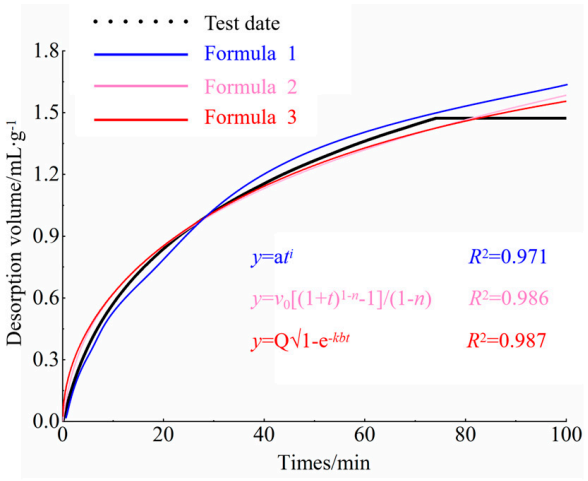
It can be seen from Figure 10 that the fitting correlation coefficients of the three equations are all above 0.9, indicating a good fitting effect. In terms of the R^2 correlation index, when the desorption equilibrium pressure was 0.74 MPa, Formula 1 displayed a lower R^2 value compared to the other two empirical formulas, suggesting a weaker fitting correlation. Conversely, the other two formulas exhibited better fitting effects. As the equilibrium pressure increased, the correlation coefficients for all formulas also increased, albeit less noticeably for Formulas 2 and 3. When Formula 1 reached 1.46 MPa, its R^2 value increased to 0.977, significantly improving the fitting degree. However, Formula 2 had an R^2 value of 0.987, and Formula 3 had an R^2 value of 0.990, indicating even better fitting results. Overall, the correlation coefficient (R^2) increased with increasing equilibrium pressure for all empirical formulas. Formula 2 showed a correlation coefficient range of 0.971–0.989, while Formula 1 had a range of 0.949–0.977. Formula 3 exhibited the smallest range of variation for its correlation coefficient, ranging from 0.979 to 0.990, resulting in the best fitting effect among the empirical formulas. The fitting results indicated that the regression coefficients of all three formulas changed with variations in the equilibrium pressure. However, the changes were significant for Formula 1, while being relatively minor for Formulas 2 and 3.

It can be seen from Figure 11 that the fitting results for the fiery coal samples were satisfactory across the three different equilibrium pressures. At an equilibrium pressure of 0.74 MPa, Formula 3 exhibited some deviation during the middle stage of gas release, while Formula 1 displayed significant deviation in the middle and late stages. Conversely, Formula 2 demonstrated the highest degree of fitting. At an equilibrium pressure of 1.06 MPa, Formula 2 exhibited the best fitting results, although Formulas 3 and 1 showed some deviation during the early and middle stages of gas dispersion. Under an equilibrium

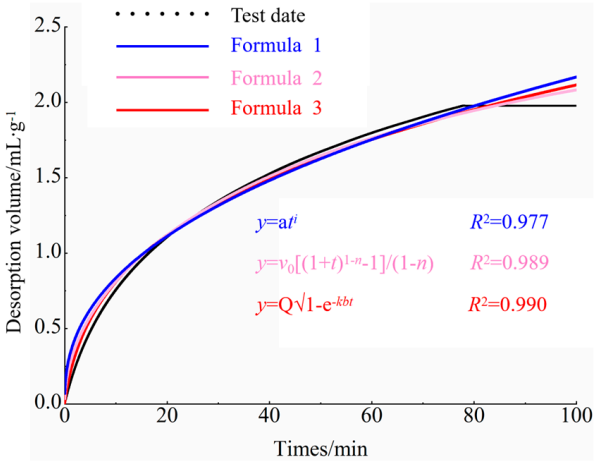
pressure of 1.46 MPa, both Formulas 3 and 1 deviated during the middle and late stages of gas release, while Formula 2 continued to display the highest degree of fitting. This suggests that Formula 2 provided a good fitting effect. Throughout the entire desorption process, the correlation coefficient of Formula 2 varied only between 0.993 and 0.998. Additionally, Formula 1 had a fitting correlation coefficient of 0.993–0.997, indicating its ability to accurately describe the diffusion process of coal samples. Considering the fitting regression coefficient, Formula 3 exhibited the smallest range of variation, implying that using Formula 3 data in different equilibrium pressure segments to calculate gas loss would result in minimal differences and greater stability.



(**a**) 0.74 MPa.



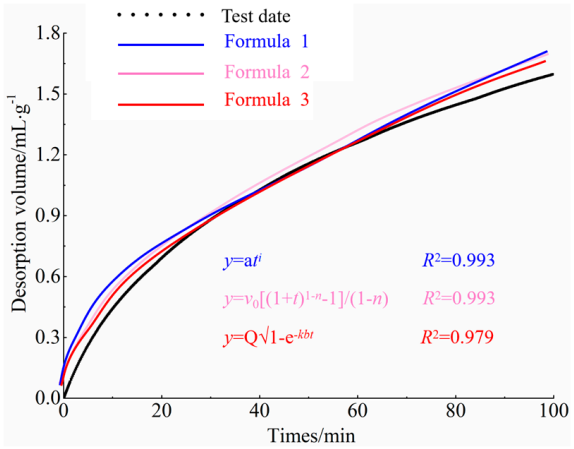
(**b**) 1.06 MPa.



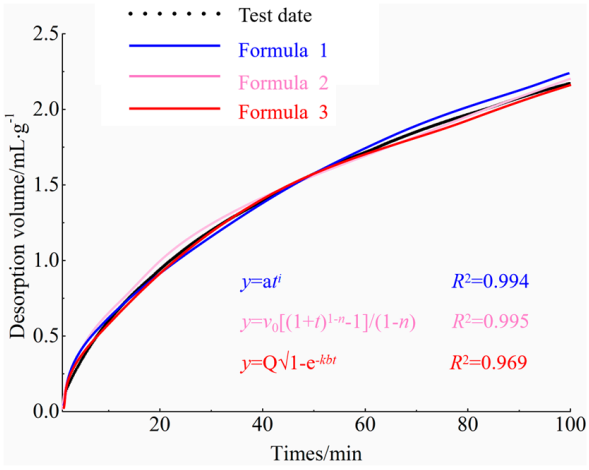
(**c**) 1.46 MPa.

Figure 10. Fitting curve for the amount of desorption in lignite. (**a**) 0.74 MPa; (**b**) 1.06 MPa; (**c**) 1.46 MPa.

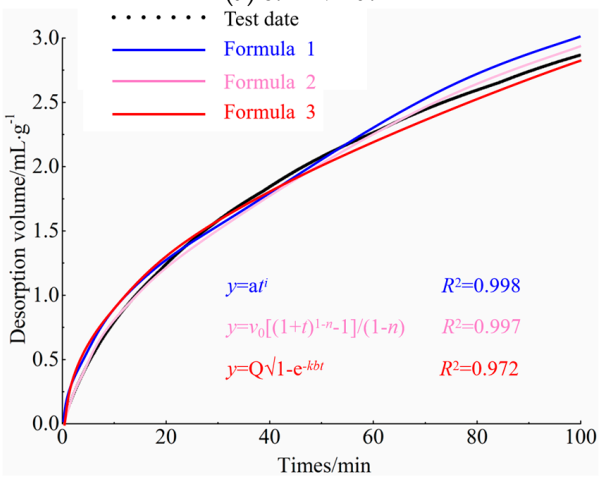
It can be seen from Figure 12 that the empirical formula displayed a good fitting effect in the early stage for the anthracite coal samples. The correlation coefficient (R^2) of the fitting equation gradually increased with increasing equilibrium pressure and then gradually decreased after reaching a certain point. The correlation coefficients obtained using Formulas 2, 1, and 3 were all greater than 0.95. However, Formula 2 consistently yielded correlation coefficients above 0.99 for the entire desorption process, reflecting a strong fitting effect.



(**a**) 0.74 MPa.



(**b**) 1.06 MPa.



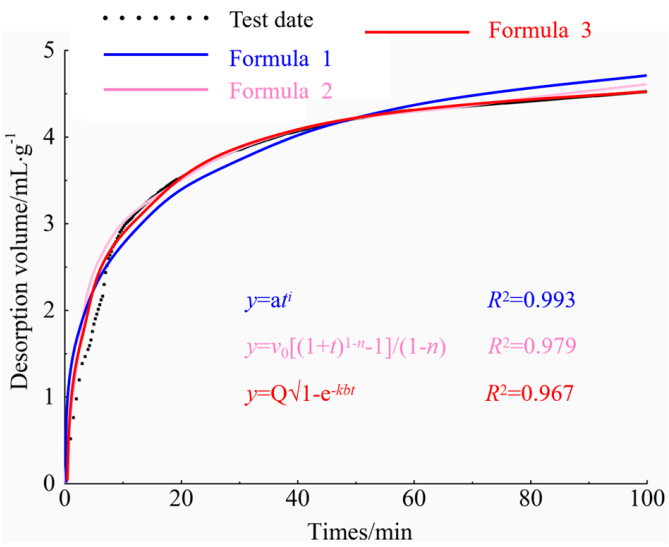
(**c**) 1.46 MPa.

Figure 11. Desorption fitting curve for fiery coal. (**a**) 0.74 MPa; (**b**) 1.06 MPa; (**c**) 1.46 MPa.

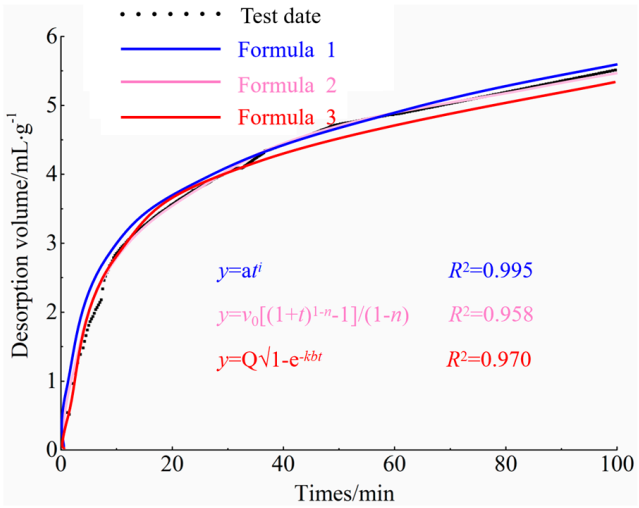
At an equilibrium pressure of 0.74 MPa, Formula 2 exhibited some deviation in the early stage, while Formula 3 showed the highest degree of fitting and Formula 1 displayed deviations during the early, middle, and late stages of gas dispersion. Under an equilibrium pressure of 1.06 MPa, Formula 2 demonstrated the highest degree of fitting, while Formulas 3 and 1 exhibited certain deviations in the early and middle stages. Similarly, under an equilibrium pressure of 1.46 MPa, Formula 2 again had the highest degree of fitting, while Formula 1 deviated during the middle and late stages of gas dispersion.

The fitting results indicate that the overall applicability of the three empirical formulas was relatively good, especially at an equilibrium pressure of 1.46 MPa. Formulas 2, 1, and 3 all achieved high correlation index values, indicating a relatively good fitting effect.

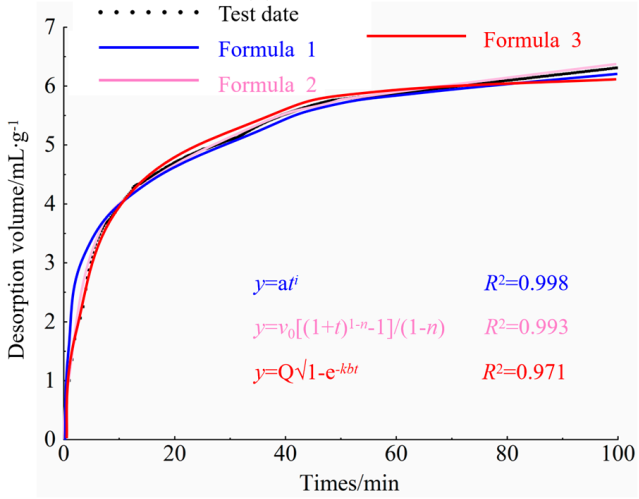
In the experiment, different classical empirical formulas were adopted to conduct a regression analysis on the experimental data obtained for desorption in three groups of coal samples under different equilibrium pressures. The three empirical fitting formulas used for anthracite yielded relatively stable correlation index values, indicating a good fitting effect. The fitting results of Formulas 2, 3, and 1 under an equilibrium pressure of 1.46 MPa were relatively ideal. For lignite, Formula 3 exhibited a relatively large correlation coefficient (R^2) with a small range of variation, indicating a better fitting effect compared to the other two empirical formulas. Additionally, for fiery coal, Formula 3 accurately described the gas release process of the coal samples.



(**a**) 0.74 MPa.



(**b**) 1.06 MPa.



(**c**) 1.46 MPa.

Figure 12. Desorption fitting curve for anthracite. (**a**) 0.74 MPa; (**b**) 1.06 MPa; (**c**) 1.46 MPa.

Building upon prior research theories, this paper scrutinizes the gas desorption and diffusion behaviors of lignite, bituminous coal, and anthracite. It employs more comprehensive mathematical formulas to fit gas desorption curves, revealing gas release patterns and applicable models for coals with varying metamorphic degrees. This analysis not only enhances comprehension of gas desorption and diffusion laws but also offers insights for predicting and preventing coal and gas outbursts. It establishes a solid foundation for accident prevention and holds practical significance for enhancing mine safety practices. Nonetheless, the study in this paper only tested three representative coal samples, which could potentially introduce deviations in the results. The author intends to conduct additional gas desorption and diffusion tests and model studies on a broader range of coal samples and ranks in future research endeavors.

5. Conclusions

(1) Coal samples with a higher degree of metamorphism exhibited a faster attainment of the desorption limit value, whereas low-rank lignite required a longer period to reach this limit. However, as the desorption time increased, the desorption rate of highly metamorphic coal samples gradually declined, resulting in a progressively slower desorption rate.

(2) As coal metamorphism increased, the rate of decline in the gas desorption rate slowed down, and the higher the degree of coal metamorphism, the greater the amount of gas desorption. The effective gas diffusion coefficient of the coal samples exhibited a strongly negative linear correlation with the degree of metamorphism, indicating that the ability of the coal samples to facilitate gas diffusion decreased as the degree of metamorphism increased.

(3) Among the three empirical fitting formulas applied to anthracite, a relatively stable correlation index was obtained, and the fitting effect was satisfactory. For an equilibrium pressure of 1.46 MPa, the fitting results for Formulas 2, 3, and 1 were relatively ideal. Formula 3 yielded a relatively high correlation coefficient (R^2) and exhibited a smaller range of coefficient variation for lignite, making it a more effective fitting formula compared to the other two. For fiery coal, Formula 3 was deemed more suitable for describing the gas desorption process of the coal samples.

Author Contributions: H.X.: Conceptualization, Data curation, Writing—original draft. X.Q.: Data curation, Formal analysis. H.W.: Funding acquisition, Methodology. Z.L.: Formal analysis. T.Y.: Formal analysis, Visualization. Y.Z.: Formal analysis. Q.J.: Formal analysis. L.J.: Formal analysis, Visualization. All authors have read and agreed to the published version of the manuscript.

Funding: This research was funded by the Natural Science Foundation of Hebei Province (E2024508006), the National Natural Science Foundation of China (52274200).

Data Availability Statement: The data used to support the findings of this study are available from the corresponding author upon request.

Conflicts of Interest: Authors Zhongqiu Liang and Yongming Zou were employed by the company CCTEG Shenyang Research Institute. The remaining authors declare that the research was conducted in the absence of any commercial or financial relationships that could be construed as a potential conflict of interest.

References

1. Li, W.; Guo, Y.; Liu, X.; Du, F.; Li, G.; Ma, Q. Failure mechanisms and reinforcement support of roadway in deep coal seam: A case study. *Eng. Fail. Anal.* **2024**, *165*, 108745. [CrossRef]
2. Clarkson, C.R.; Bustin, R.M. The effect of pore structure and gas pressure upon the transport properties of coal: A laboratory and modeling study. 2. Adsorption rate modeling. *Fuel* **1999**, *78*, 1345–1362. [CrossRef]
3. Guo, Y.; Wang, K.; Du, F.; Guo, H.; Li, K.; Wang, Y. Mechanical-permeability characteristics of composite coal rock under different gas pressures and damage prediction model. *Phys. Fluids* **2024**, *36*, 036615. [CrossRef]
4. Wang, K.; Zhao, E.; Guo, Y.; Du, F.; Ding, K. Effect of loading rate on the mechanical and seepage characteristics of gas-bearing coal–rock and its mechanical constitutive model. *Phys. Fluids* **2024**, *36*, 026606. [CrossRef]
5. Guo, Y.; Liu, X.; Li, W.; Du, F.; Ma, J.; Qian, R.; Huo, N. Research on abutment stress distribution of roof-cutting coalface: Numerical simulation and field measurement. *Geomech. Geophys. Geo-Energ Geo-Resour.* **2024**, *10*, 86. [CrossRef]
6. Yang, T.; Xu, T.; Liu, H.; Tang, C.; Shi, B.; Yu, Q. Stress-damage-flow coupling model and its application to pressure relief coal bed methane in deep coal seam. *Int. J. Coal Geol.* **2011**, *86*, 357–366. [CrossRef]
7. Pan, Z.; Connell, L.D.; Camilleri, M.; Connelly, L. Effects of matrix moisture on gas diffusion and flow in coal. *Fuel* **2010**, *89*, 3207–3217. [CrossRef]
8. Wang, K.; Guo, Y.; Du, F.; Dong, H.; Xu, C. Effect of the water injection pressure on coal permeability based on the pore-fracture fractal characteristics: An experimental study. *Greenh. Gases-Sci. Technol.* **2022**, *12*, 136–147. [CrossRef]
9. Si, G.; Jamnikar, S.; Lazar, J.; Shi, J.Q.; Durucan, S.; Korre, A.; Zavšek, S. Monitoring and modelling of gas dynamics in multi-level longwall top coal caving of ultra-thick coal seams, Part II: Numerical modelling. *Int. J. Coal Geol.* **2015**, *144*, 58–70. [CrossRef]
10. Li, J.; Lu, S.; Zhang, P.; Cai, J.; Li, W.; Wang, S.; Feng, W. Estimation of gas-in-place content in coal and shale reservoirs: A process analysis method and its preliminary application. *Fuel* **2020**, *259*, 116266. [CrossRef]
11. Gao, T.; Zhao, D.; Wang, C.; Feng, Z. Energy variation in coal samples with different particle sizes in the process of adsorption and desorption. *J. Pet. Sci. Eng.* **2020**, *188*, 106932. [CrossRef]
12. Li, X.; Li, Z.; Ren, T.; Nie, B.; Xie, L.; Huang, T.; Bai, S.; Jiang, Y. Effects of particle size and adsorption pressure on methane gas desorption and diffusion in coal. *Arab. J. Geosci.* **2019**, *12*, 794. [CrossRef]

13. Karacan, C.Ö.; Esterhuizen, G.S.; Schatzel, S.J.; Diamond, W.P. Reservoir simulation based modeling for characterizing longwall methane emissions and gob gas venthole production. *Int. J. Coal Geol.* **2007**, *71*, 225–245. [CrossRef]
14. Gao, Y.; Lin, B.; Yang, W.; Li, Z.; Pang, Y.; Li, H. Drilling large diameter crossmeasure boreholes to improve gas drainage in highly gassy soft coal seams. *J. Nat. Gas. Sci. Eng.* **2015**, *26*, 193–204. [CrossRef]
15. Xu, S.; Hu, E.; Li, X.; Xu, Y. Quantitative Analysis of Pore Structure and Its Impact on Methane Adsorption Capacity of Coal. *Nat. Resour. Res.* **2020**, *30*, 605–620. [CrossRef]
16. Wang, G.; Guo, Y.; Wang, P.; Li, W.; Wu, M.; Sun, L.; Cao, J.; Du, C. A new experimental apparatus for sudden unloading of gas-bearing coal. *Bull. Eng. Geol. Environ.* **2020**, *79*, 857–868. [CrossRef]
17. Mora, C.A.; Wattenbarger, R.A. Analysis and verification of dual porosity and CBM shape factors. *J. Can. Pet. Technol.* **2009**, *48*, 17–21. [CrossRef]
18. Karacan, C.Ö. Analysis of gob gas venthole production performances for strata gas control in longwall mining. *Int. J. Rock. Mech. Min. Sci.* **2015**, *79*, 9–18. [CrossRef]
19. Wang, G.; Guo, Y.; Du, C.; Sun, L.; Liu, Z.; Wang, Y.; Cao, J. Experimental Study on Damage and Gas Migration Characteristics of Gas-Bearing Coal with Different Pore Structures under Sorption-Sudden Unloading of Methane. *Geofluids* **2019**, *2019*, 7287438. [CrossRef]
20. Nie, B.S.; Yang, T.; Li, X.C.; Li, L.; Lu, H. Research on diffusion of methane in coal particles. *J. China Univ. Min. Technol.* **2013**, *42*, 975–981.
21. Li, Y.; Zhang, Y.; Zhang, L.; Hou, J. Characteristics on pore structure of tectonic coals based on the methods of mercury intrusion, carbin dioxide adsorption and nitrogen adsorption. *J. China Coal Soc.* **2019**, *44*, 1188–1196.
22. Saghafi, M.; Mohamad Rezaee, M. The effect of coal rank on coalbed methane desorption kinetics: A review and case study. *Fuel* **2018**, *215*, 602–615.
23. Gasparik, M.; Sykorova, I. Influence of coal rank on coalbed methane desorption characteristics. *J. Nat. Gas Sci. Eng.* **2019**, *66*, 1–9.
24. Kusuma, M.I. Investigation of the effect of coal rank on coalbed methane desorption using molecular dynamics simulation. *J. Nat. Gas Sci. Eng.* **2018**, *57*, 9–18.
25. Kang, Z.; Li, X.; Li, W.; Zhao, J. Experimental investigation of methane adsorption/desorption behavior in coals with different coalbody structure and its revelation. *J. China Coal Soc.* **2018**, *43*, 1400–1407.
26. Hu, B.; Cheng, Y.; Wang, L. Study on porous structure and gas diffusion characteristics of primary structure coal and tectonic coal. *Coal Sci. Technol.* **2018**, *46*, 103–107.
27. *GB/T 212-2008*; Methods for Industrial Analysis of Coal. China Planning Press: Beijing, China, 2008.
28. *GB/T 40485-2021*; Image Analysis for Automatic Determination of Vitrinite Random Reflectance of Coal. China Planning Press: Beijing, China, 2021.
29. *GB/T 21650.1-2008*; Pore Size Distribution and Porosity of Solid Materials by Mercury Porosimetry and Gas Adsorption—Part 1: Mercury Porosimetry. China Planning Press: Beijing, China, 2008.
30. *GB/T 19560-2008*; Experimental Method of High-Pressure Isothermal Adsorption to Coal. China Planning Press: Beijing, China, 2008.

Disclaimer/Publisher's Note: The statements, opinions and data contained in all publications are solely those of the individual author(s) and contributor(s) and not of MDPI and/or the editor(s). MDPI and/or the editor(s) disclaim responsibility for any injury to people or property resulting from any ideas, methods, instructions or products referred to in the content.